Characterisation of Transverse Matrix Cracks in Composite Materials Using Fibre Bragg Grating Sensors

Rajabzadeh, Aydin; Heusdens, Richard; Hendriks, Richard C.; Groves, Roger M.

DOI
10.1109/JLT.2019.2919339

Publication date
2019

Document Version
Final published version

Published in
Journal of Lightwave Technology

Characterisation of Transverse Matrix Cracks in Composite Materials Using Fibre Bragg Grating Sensors

Aydin Rajabzadeh, Richard Heusdens, Richard C. Hendriks, and Roger M. Groves

***Abstract*—In this paper, we propose a novel approach to characterise barely visible transverse matrix cracks in composite structures using fibre Bragg grating (FBG) optical sensors. Matrix cracks are one of the most prevalent types of damage in composite structures, and detecting them in the internal layers of composites has remained a challenge. In this paper, we will show that the formation of cracks in the internal layers of composite structures alters the side-lobes of the reflection spectra of FBG sensors by adding new harmonics to them. We argue that the spread and the location of these harmonics depends on both the mechanical properties of the composite material and the location of the crack along the length of the FBG sensor. Via computer simulations and experimental measurements, we validate our hypotheses, and the results are in agreement with our model.**

***Index Terms*—Barely visible damage, composites, FBG, fiber Bragg gratings, matrix cracks, reflection spectrum, smart structures, structural health monitoring (SHM).**

I. Introduction

FIBRE Bragg grating (FBG) sensors are optical fibre based sensors that are produced by creating a modulation in the refractive index of the core of the fibre for lengths usually in the order of a few millimetres to a few centimetres [1]. The small diameter of these sensors allows them to be embedded between the layers of composite laminates without severely changing the mechanical properties of the composite structure [2]. This makes FBG sensors interesting for structural health monitoring of composite materials. FBG sensors can provide insight into the internal layers of composites, including internal strain and temperature measurements [2], monitoring the behaviour of composites during the curing process [3], and for the detection of cracks and damages [4]–[6]. Although the main application of FBG sensors has been in the field of point strain and temperature measurements [1], [7], in the last few decades several studies have been carried out on the subject of damage detection in composites, including the most prevalent types of damages in composites such as delamination and matrix cracks.

The current study belongs to the latter category, with a focus on the characterisation of barely visible matrix cracks within the internal layers of composites that occur along the length of embedded FBG sensors. Within this framework, several studies have been conducted in the past few decades. Although most of these methods can potentially distinguish between a uniform and a non-uniform stress field over the composite panel, they lack the capability of differentiating a composite part that is affected by cracks from other sorts of non-uniform stress fields, transverse loads and birefringence effects. In [8], chirped FBG sensors were used for crack detection. It was argued that the formation of cracks along the length of such chirped FBG sensors will result in the emergence of dips and valleys in the reflection spectra. In [9] the case of transversal crack formation around holes in composite structures was investigated. In [10], Chambers *et al.* argued that the shift of the Bragg wavelength of FBG sensors (or equivalently a change in strain) is a measure good enough to detect impact damages and cracks. In [6] and [11] Okabe *et al.* argued that there is an empirical relation between the width of the FBG reflection spectra and the transverse crack density. Based on the modelling that will be presented in this paper, we will show that the argumentation on the empirical relation between the width of the FBG reflection spectra and the transverse crack density given in [6] and [11] is indeed correct. However, we will show that a widened FBG reflection spectrum can also be associated with non-uniform stress fields that are not related to transversal cracks. The width of the FBG reflection spectrum can thus not unambiguously be used to indicate the presence of transversal cracks.

In this study, expanding work first presented at the 26th Optical Fiber Sensors Conference, OFS-26 [12], we will analyse the effect of transverse cracks on FBG reflection spectra from a new perspective. We will present a mathematical model for the analysis of FBG reflection spectra from sensors that are affected by transverse cracks, and we will show that the

Manuscript received January 10, 2019; revised May 18, 2019; accepted May 23, 2019. Date of publication May 28, 2019; date of current version September 18, 2019. This work is part of the TKI Smart Sensing for Aviation Project, supported in part by the Dutch Ministry of Economic Affairs under the Topsectoren policy for High Tech Systems and Materials, in part by the industry partners Airbus Defence and Space, Fokker Technologies—GKN Aerospace, Royal Schiphol Group, and in part by the H2020 project Extreme GA636549. *(Corresponding author: Aydin Rajabzadeh.)*

A. Rajabzadeh is with the Circuits and Systems Group, Electrical Engineering Faculty, Delft University of Technology, 2628 Delft, The Netherlands, and also with the Structural Integrity and Composites Group, Aerospace Engineering Faculty, Delft University of Technology, 2628 Delft, The Netherlands (e-mail: a.rajabzadehdizaji@tudelft.nl).

R. Heusdens and R. C. Hendriks are with the Circuits and Systems Group, Electrical Engineering Faculty, Delft University of Technology, 2628 Delft, The Netherlands (e-mail: r.heusdens@tudelft.nl; r.c.hendriks@tudelft.nl).

R. M. Groves is with the Structural Integrity and Composites Group, Aerospace Engineering Faculty, Delft University of Technology, 2629 Delft, The Netherlands (e-mail: r.m.groves@tudelft.nl).

Color versions of one or more of the figures in this paper are available online at http://ieeexplore.ieee.org.

Digital Object Identifier 10.1109/JLT.2019.2919339

information regarding the formation of cracks lies within the side-lobes of these spectra. We will substantiate our hypotheses with both computer simulations and experimental measurements on composite coupons.

II. FBG Reflection Spectra Under Non-Uniform Strain Fields

One of the most interesting properties of uniform FBG sensors is that under uniform strain distributions, the shift of the peak wavelength of the reflection spectrum (also known as the Bragg wavelength) depends linearly on the amount of strain applied to the sensor [1]. This linear relationship is characterised by the following equation:

$$\Delta\lambda_B = k_s s, \tag{1}$$

where k_s is a constant factor that depends on the physical properties of the sensor, and s is the amount of uniform strain applied over the length of the sensor. Under such uniform strain fields, the reflection spectrum has a close to symmetrical shape, with one main-lobe with a high amplitude, and several side-lobes with smaller amplitudes. However, when the sensor is subject to non-uniform strain fields, the reflection spectrum will take a more complicated form with multiple peaks and a broadened width. In that case, Eq. (1) does not have a clear meaning anymore. As an example, in [13] we showed that deviating from the average strain by as much as 150 $\mu\epsilon$ results in the FBG reflection spectrum to be asymmetrical, and to have side-lobes with more than half the amplitude of the main peak. In this section, we will investigate this effect on the overall FBG reflection spectrum of two categories of non-uniform strain fields, namely smoothly varying strain fields and sharply varying strain fields. We will argue that each of these cases has a different effect on the frequency content of the side-lobes of the FBG reflection spectrum.

In [13] we proposed an approximated transfer matrix model (ATMM) for analysis of FBG reflection spectra under non-uniform strain fields. The ATMM, which is based on the classic transfer matrix model (TMM) [14], discretises the length L of the sensor into M smaller piece-wise uniform segments each with a length of Δz, and assumes a staircase approximation of the strain field over the length of the sensor. In such conditions, we can assume that (1) is valid for each of these individual segments. The ATMM describes the interaction of the forward and backward electric field amplitude at each segment, denoted by A_i and B_i respectively, via the following relations

$$\begin{pmatrix} A_i \\ B_i \end{pmatrix} = F_i \begin{pmatrix} A_{i-1} \\ B_{i-1} \end{pmatrix},$$

where

$$F_i = \begin{pmatrix} e^{-j(\alpha-\alpha_i)} & -j\kappa_i \Delta z\,\mathrm{sinc}(\alpha-\alpha_i) \\ j\kappa_i \Delta z\,\mathrm{sinc}(\alpha-\alpha_i) & e^{j(\alpha-\alpha_i)} \end{pmatrix}. \tag{2}$$

Here, κ_i is the coupling coefficient between the forward and backward electric field amplitude at segment i, with

$$\alpha = \frac{2\pi n_{\text{eff}} \Delta z}{\lambda} \text{ and } \alpha_i = \frac{2\pi n_{\text{eff}} \Delta z}{\lambda_{B_i}}. \tag{3}$$

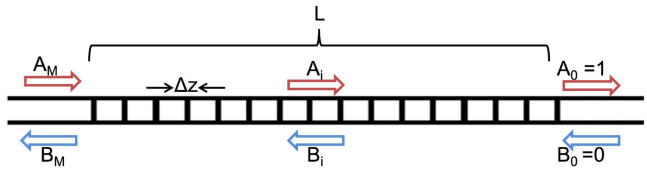

Fig. 1. Schematic view of the FBG structure.

In Eq. (3), n_{eff} is the effective refractive index of the core, λ is the wavelength region under investigation, and λ_{B_i} is the local Bragg wavelength of segment i. Therefore, α can be considered as a scaled frequency and α_i as the Bragg frequency of segment i. Fig. 1 shows a schematic representation of the FBG structure under non-uniform stress fields. The relationship between the electric field amplitudes from the first and the last segment can be characterised as

$$\begin{pmatrix} A_M \\ B_M \end{pmatrix} = F \begin{pmatrix} A_0 \\ B_0 \end{pmatrix}, \text{in which } F = \prod_{i=1}^{M} F_i.$$

Considering the boundary conditions for the above equations at the last segment (full transmission of the incident light ($A_0 = 1$) and no reflection from the rest of the sensor ($B_0 = 0$)), the reflection spectrum can be calculated as

$$R(\lambda) = \left|\frac{B_M}{A_M}\right|^2 = \left|\frac{F_{21}}{F_{11}}\right|^2,$$

where F_{21} and F_{11} are entries of the composite matrix F. For the analysis of this paper, we are interested in a closed form expression for the FBG reflection spectrum. This can be achieved by approximating the elements of the composite matrix F, such that, the reflection spectrum can be approximated as [13]

$$R(\lambda) \overset{(a)}{\approx} \left| \sum_{i=1}^{M} \kappa_i \Delta z\,\mathrm{sinc}(\alpha-\alpha_i) e^{-j\left((M-2i+1)\alpha + \sum_{k<i}\alpha_k - \sum_{k>i}\alpha_k\right)} \right|^2 \tag{4}$$

$$\overset{(b)}{=} \left| \sum_{i=1}^{M-1} \overbrace{(\xi_i - \xi_{i+1})}^{\zeta_i} e^{-j\left((M-2i)\alpha + \sum_{k\le i}\alpha_k - \sum_{k>i}\alpha_k\right)} + \left(\xi_M e^{jM(\alpha-\bar{\alpha})} - \xi_1 e^{-jM(\alpha-\bar{\alpha})}\right) \right|^2, \tag{5}$$

where (a) is obtained by neglecting the products of the sinc functions with the low amplitudes in the F_{11} and F_{21} elements (see [13]), and (b) follows by re-arranging the terms in (4). Further,

$$\xi_i = \frac{\kappa_i \Delta z}{2j(\alpha-\alpha_i)}. \tag{6}$$

The approximation in (4) is most accurate in the side-lobes of the reflection spectrum [13]. To analyse the effect of different kinds of strain fields on the reflection spectrum, we will focus on the ζ_i terms given in (5) as $\zeta_i = \xi_i - \xi_{i+1}$.

From (5) it can be seen that the reflection spectrum is a function of the local Bragg frequencies (α_i), that are a function of the strain field over the length of the sensor, via the following relation [13]

$$\alpha_i = \frac{\rho}{\lambda_i} = \frac{\rho}{\bar{\lambda}_B + \Delta\lambda_i} \approx \bar{\alpha} - \frac{\rho}{\bar{\lambda}_B^2}\Delta\lambda_i = \bar{\alpha} - k_s\frac{\rho}{\bar{\lambda}_B^2}s_i, \quad (7)$$

where $\rho = 2\pi n_{\text{eff}}\Delta z$, and $\bar{\lambda}_B^2$ is the mean of all Bragg wavelengths along the length of the sensor, and the s_i's are the local strain values of each segment of the FBG model. Indeed, (7) suggests that a linear shift in the local Bragg wavelengths (or a shift in strain along the FBG length) results in a linear shift in the local Bragg frequencies, i.e., the α_i's.

When the strain field along the length of the FBG sensor is smooth (no discontinuity along the length of the FBG sensor), the ζ_i parameters will be small and the first $M-1$ terms in (5) can be neglected, so that the side-lobes of the reflection spectrum can be approximated by

$$R(\lambda) \approx (\kappa L)^2 \,\text{sinc}^2\left(M(\alpha - \bar{\alpha})\right) + (\xi_M - \xi_1)^2, \quad (8)$$

where $\bar{\alpha} = \sum(\alpha_i)/M$, and $L = M\Delta z$ is the sensor length. In other words, the side-lobes of the reflection spectra will only have one dominant oscillating frequency. On the other hand, if the strain field is not smooth and has sharp variations along the FBG length, the ζ_i variables will not be negligible anymore and additional harmonics will appear.

In the next section, we will analyse the effect of transverse cracks on the strain field along the sensor length, the highly non-uniform strain distribution they impose on the FBG sensor, and the consequent large ζ_i values at the crack locations. In Section (IV) we will investigate the effect of such large ζ_i values on the frequency content of the side-lobes of the FBG reflection spectra.

III. Strain Field Under Transverse Cracks

In this section, we will use the McCartney's theory to characterise the stress behaviour of composite materials with transverse matrix cracks in their internal layers. We will see that under transverse cracks, the strain distribution along the FBG length will be highly non-uniform, with its peaks located at the cracks locations.

Consider an FBG sensor embedded between the layers of a healthy unidirectional carbon fibre reinforced plastic (CFRP) composite structure. Due to the brittle nature of the matrix material, under fatigue or impact damages, matrix cracks could form in the internal layers of composite. Based on McCartney's theory [15] and using the formulations derived in [16], for a composite material with given mechanical properties, the strain distribution along the length of an embedded optical fibre can be analytically calculated. The schematic diagram of a composite structure and its dimensions is shown in Fig. 2(a) and an FBG sensor with a length of 10 mm embedded between two layers with orthogonal unidirectional layer direction is shown in Fig. 2(b).

Based on McCartney's theory, in the presence of transversal cracks in the middle layer of the composite, the strain field in the 0° layer along the length of the FBG has the form given in Fig. 3. We will use strain distributions of this form in Section IV to characterise the FBG reflection spectra. The shape of the strain peaks along the length of the sensor, their amplitude, and their width depends on the axial stress, the physical dimensions and the mechanical properties of the composite structure [15]. It is noteworthy that McCartney's theory is derived with the assumption that the transversal cracks are equally spaced. In reality that is generally not the case, but the effect of this non-uniformity in the distribution of cracks on the strain distribution is negligible [6].

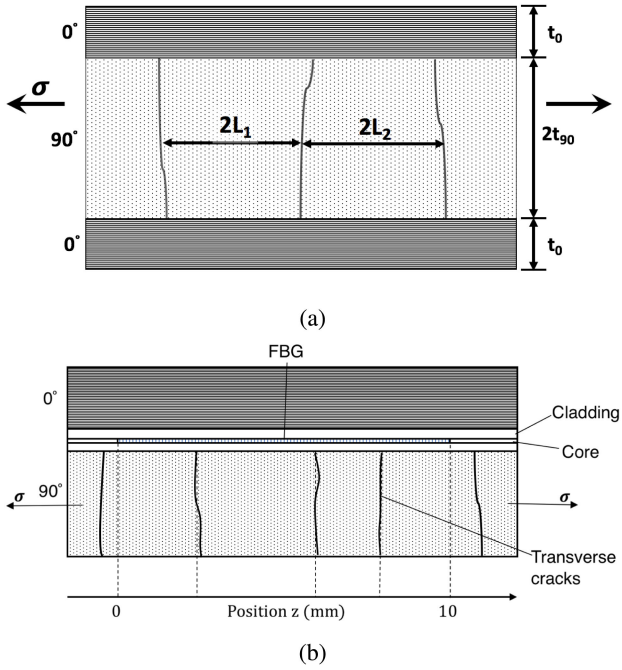

Fig. 2. (a): A schematic of the cross section of the unidirectional composite structure affected by transverse cracks in its internal layers (b): The position of the FBG sensor between the layers of the composite structure.

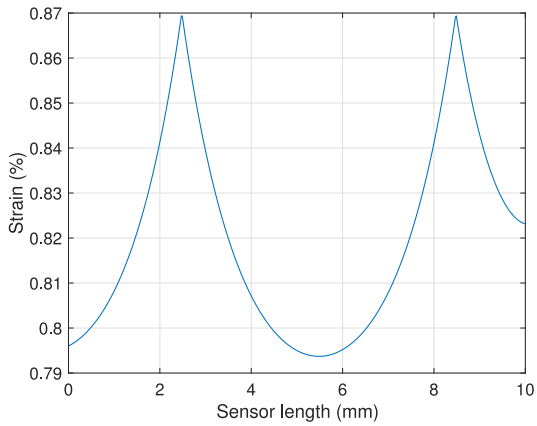

Fig. 3. The strain distribution along the FBG length embedded between the layers of a carbon fibre composite structure and affected by two transverse cracks, calculated using McCartney's theory at $\sigma = 550$ MPa.

IV. FBG Reflection Spectra Under Transverse Cracks

In Section II it was mentioned that when we have sharp strain changes along the length of the FBG sensor, the first terms in Eq. (5) are not negligible anymore. A particular example of such strain fields is when the sensor is in contact with transverse cracks in composite structures (similar to Fig. 3). Suppose there are N arbitrarily distributed cracks along the FBG length located at segments t_p, $p = 1, 2, ..., N$. In this case, the largest changes of the strain field are expected at the boundaries of each segment t_p. Consequently, the largest values of the ζ_i parameters will be at the boundaries of segment t_p as well. Therefore, Eq. (5) can be rewritten as

$$R_c(\lambda) \approx \Bigg| \sum_{i\in\mathcal{I}_c} \zeta_i e^{-j\left((M-2i)\alpha+\sum_{k\le i}\alpha_k-\sum_{k>i}\alpha_k\right)} + \sum_{i\in\mathcal{I}} \zeta_i e^{-j\left((M-2i)\alpha+\sum_{k\le i}\alpha_k-\sum_{k>i}\alpha_k\right)} + \xi_M e^{jM(\alpha-\bar{\alpha})} - \xi_1 e^{-jM(\alpha-\bar{\alpha})} \Bigg|^2, \tag{9}$$

where $\mathcal{I} = \{t_1 - 1, t_1, t_2 - 1, t_2, ..., t_N - 1, t_N\}$, and $\mathcal{I}_c = \Omega \setminus \mathcal{I}$ is the complement of the set $\mathcal{I}$ in $\Omega = \{1, 2, ..., M\}$. Note that in the case of having both the magnitude and phase spectrum, one can take the Fourier transform of the side-lobes of the reflection spectrum where each of the non-negligible exponential terms in (9) will be translated into a unique peak in the Fourier domain. In that case, we can have an exact localisation of the transverse cracks along the FBG length. However, since practically the most convenient methods of FBG interrogation only have access to the magnitude of this spectrum, we will only focus on the amplitude of the reflection spectrum in this paper.

In Eq. (9), the largest contribution of the ζ_i terms to the amplitude happen due to the second summation (corresponding with $i = t_p - 1, t_p$). With that in mind, Eq. (9) can be approximated as

$$R_c(\lambda) \approx \sum_{i=1}^{M-1} |\zeta_i|^2 + \sum_{i,k\in\mathcal{I}}\sum \zeta_i\zeta_k^* e^{j\left((2i-2k)\alpha+\theta_k-\theta_i\right)} + \sum_{i\in\mathcal{I}} 2\,\mathrm{Re}[\zeta_i\zeta_M^*]\cos\left((2M-2i)\alpha+\theta_i-M\bar{\alpha}\right) - \sum_{i\in\mathcal{I}} 2\,\mathrm{Re}[\zeta_i\zeta_1^*]\cos\left((2i)\alpha-\theta_i-M\bar{\alpha}\right) + R_r + R_s, \tag{10}$$

where $\theta_i = \sum_{k\le i}\alpha_k - \sum_{k>i}\alpha_k$, R_s is the reflection spectrum for smooth strain fields given in (8), and R_r is the summation of the remaining terms with lower amplitudes than the ones mentioned in (10), which are the cross terms resulting from the first summation term in (9). As seen from (10), the formation of each transverse crack at location t along the length of the FBG model results in the emergence of new harmonics at the angular frequencies $\omega = 2M - 2t$ and $\omega = 2t$. Additionally, for every two cracks along the FBG length at locations i and k, there will be a non-negligible cross term with oscillation frequency of $\omega = 2(i - k)$. Furthermore, it can be seen from (10) that for each crack at segment t_p, each summation term consists of pairs of harmonics corresponding with $i = \{t_p - 1, t_p\}$ (associated with large strain changes before and after the crack). Consequently, the emerging harmonics due to these consecutive segments are only separated by a frequency distance of $\omega = 2$. Due to the decaying nature of the ζ_i terms in the α domain, the harmonics associated with each of these segment pairs overlap in the Fourier domain.

In order to analyse these new emerging harmonics, we can take the Fourier transform of the side-lobes of the FBG reflection spectrum when the FBG sensor is in contact with transverse cracks. However, using a rectangular window will result in spectral leakage in the Fourier domain. In order to resolve this problem, and to also avoid the ambiguity of defining a proper range for the side-lobes, we propose replacing the rectangular window with a Hann window [17]. In this paper, the lower bound of the window is chosen to be at the centre of mass of the reflection spectrum, given by

$$\lambda_{B_c} = \frac{\int_\lambda \lambda R(\lambda)\mathrm{d}\lambda}{\int_\lambda R(\lambda)\mathrm{d}\lambda}, \tag{11}$$

where λ is the wavelength region that covers the reflection spectrum. The upper bound of the window is case dependent and is set by the user. It should cover the wavelength region where the side-lobes' amplitudes are above the noise level. After applying this window (w), we take the Fourier transform of Eq. (10), resulting in

$$\mathcal{F}\{R_c\} \approx \mathcal{F}\{R_r w\} + \mathcal{F}\{R_s w\} + \sum_{i=1}^{M}\mathcal{F}\{|\zeta_i|^2 w\} \tag{12a}$$

$$+ 4\sum_{i,k\in\mathcal{I},\, i<k} \Psi_{i,k}(\omega \mp (2i-2k)) e^{\pm(\theta_k-\theta_i)} \tag{12b}$$

$$+ 4\sum_{i\in\mathcal{I}} \Psi_{i,M}(\omega \mp (2M-2i)) e^{\pm(\theta_i-M\bar{\alpha})} \tag{12c}$$

$$- 4\sum_{i\in\mathcal{I}} \Psi_{i,1}(\omega \mp 2i) e^{\pm(-\theta_i-M\bar{\alpha})}, \tag{12d}$$

where $\Psi_{i,j}(\omega \mp (2i-2j)) = \mathcal{F}\{\mathrm{Re}[\zeta_i\zeta_j^*]w\} * \delta(\omega \mp (2i-2j))$, and $*$ denotes the convolution operator. Based on equations (12a) through (12d), a single peak in the strain distribution results in 4 new peaks in the Fourier domain in (12c) and (12d) (plus 6 other peaks that overlap with already existing harmonics), and two cross terms that emerge for each pair of peaks in the strain distribution in (12b). Out of these harmonics, the harmonics at $\omega = \{0, \pm 2M\}$ (included in the $\mathcal{F}\{R_s\}$ term) are always present and are independent of the strain field to which the sensor is subjected. Note that there are several other harmonics within the $\mathcal{F}\{R_r\}$ term in Eq. (12a) as well. However, since in the transverse crack scenario, the amplitude of all the ζ_i for $\forall\, i \neq \{t_p - 1, t_p\}$ terms are smaller than ζ_{t_p-1} and ζ_{t_p}, the corresponding $\mathcal{F}\{\psi_i w\}$ terms will also have smaller amplitudes and will not form new peaks.

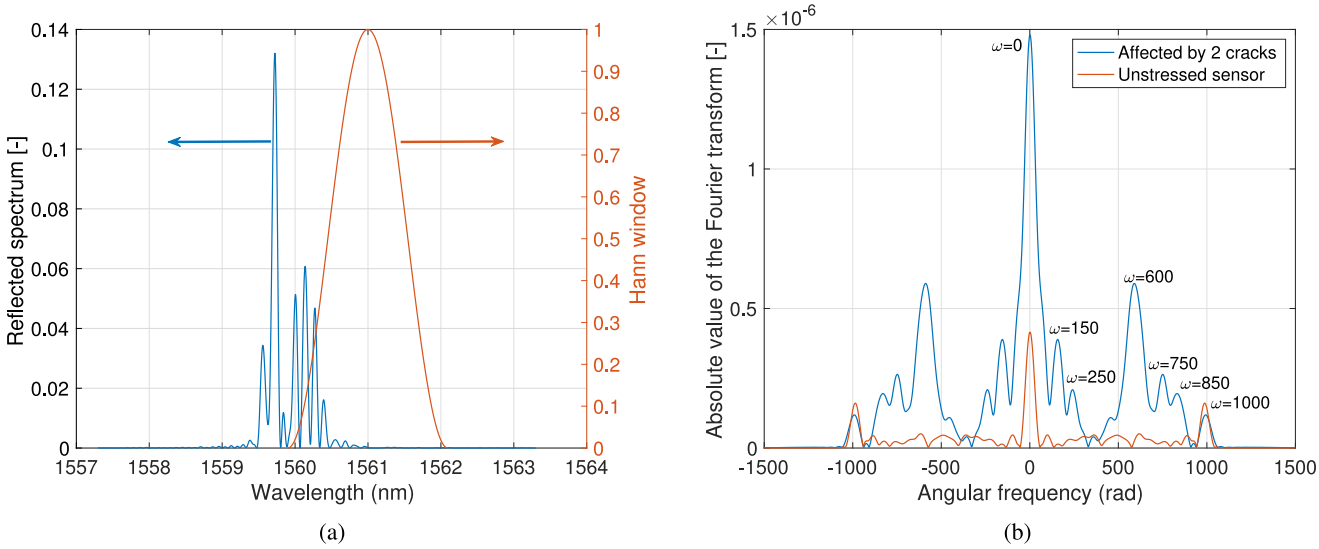

Fig. 4. (a): Reflection spectrum of a sensor near two cracks and the scaled Hann window. (b): Fourier transform of the windowed side-lobes for both stressed and unstressed sensors.

TABLE I
MECHANICAL PROPERTIES OF THE COMPOSITE STRUCTURE (USING THE DATA IN THE DATASHEET OF THE HEXPLY 8552 AND [18])

Material		Carbon fibre	Glass fibre
Elastic moduli (GPa)	E_0	148	36.5
	E_{90}	9.57	12.6
Shear modulus (GPa)	G_{xz}	5.6	3.9
Dimensions (mm)	t_0	0.732	0.34
	t_{90}	1.46	0.51
Axial stress (MPa)	σ	550	250

The FBG sensor is embedded in the 0° Layer, in the proximity of the 90° layer and the cracks.

As mentioned before in this section, for N transverse cracks along the FBG length, there will be $2(\binom{N}{2} + 2N)$ new harmonics in the Fourier domain with relatively large amplitudes. In the case that the number of transverse cracks along the FBG length increases, it is likely that due to the limited resolution, several of the new peaks in the Fourier domain appear to be overlapping. This makes the localisation of the cracks challenging for the cases where we have more than one or two cracks along the length of the sensor, without any prior knowledge about the strain field. However, for early stages of crack formation (having one or two cracks along FBG length), this information can be used to precisely localise the cracks as well (except for a reflection line of symmetry ambiguity). Furthermore, by choosing FBG sensors with shorter lengths, the spatial resolution can be improved.

In order to visualise the analyses, we will focus on transverse crack formation in two different types of composites, namely carbon fibre and glass fibre composites. The mechanical and physical properties of the materials that we used in this study are listed in Table I.

Consider the strain field given in Fig. 3 in a carbon fibre composite material, where the transverse cracks are located at $z = 2.5$ mm and at $z = 8.5$ mm from the start of a simulated FBG sensor with a total length of 10 mm and a nominal Bragg wavelength of 1550 nm. The calculated reflection spectrum in response to the FBG sensor being subjected to such a strain field is shown in Fig. 4. The FBG model was assumed to have $M = 500$ segments, therefore, the location of the crack will lie within the $t_1 = 125$'th and $t_2 = 425$'th segments. In all the computer simulations in this paper, we considered an additive zero mean Gaussian noise on the ac amplitude of the refractive index of the core (SNR = 18 dB), and also on the grating period of the FBG structure. This additive noise could lead to the emergence of new arbitrary peaks in the Fourier domain between $\omega = 0$ rad and $\omega = 1000$ rad angular frequencies, but for an unstressed sensor, they have much lower amplitudes than those resulting from transverse cracks. From equations (12b) through (12d) we expect to see new peaks emerging at angular frequencies $\omega = \{0, \pm 150, \pm 250, \pm 600, \pm 750, \pm 850, \pm 1000\}$ rad.

As seen from Fig. 4, new peaks have emerged in the Fourier transform of the side-lobes of the reflection spectra at the predetermined frequencies, which are more noticeable in the stressed sensor signal when compared with the healthy unstressed sensor signal (Fig. 4(b)).

In a second computer simulation, we considered a glass fibre composite material, of which the physical properties are given in Table I. In this example we assigned the composite structure to have 6 cracks along the length of the FBG sensor. The resulting reflection spectrum, and the Fourier transform of its side-lobes, are given in Fig. 5. Based on the discussions, for 6 transverse cracks, we expect to have 54 new peaks in the Fourier domain. However, due to the overlap of several of these peaks, there are only 14 peaks visible in the figure, which mostly correspond with cross terms that are defined in (12b) (due to their relatively higher amplitudes).

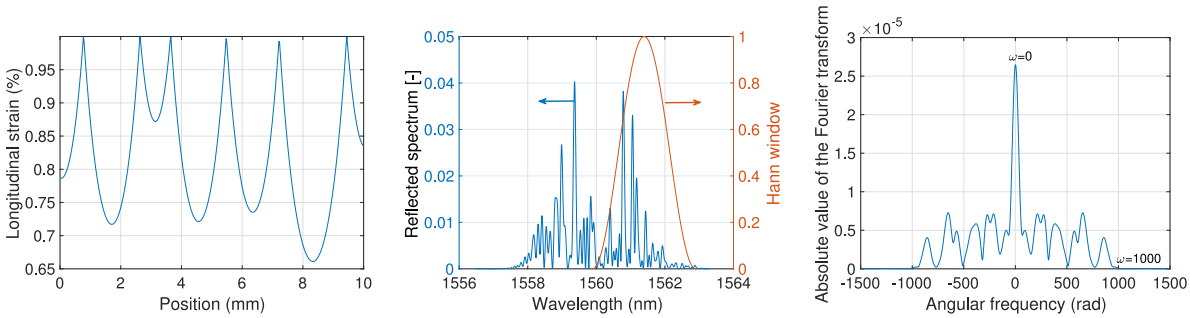

Fig. 5. (a): Strain distribution along the length of the sensor when subjected to 6 transverse cracks, at $\sigma = 250$ MPa (b): Reflection spectrum of a sensor near six cracks and the scaled Hann window. (b): Fourier transform of the windowed side-lobes of the reflection spectrum.

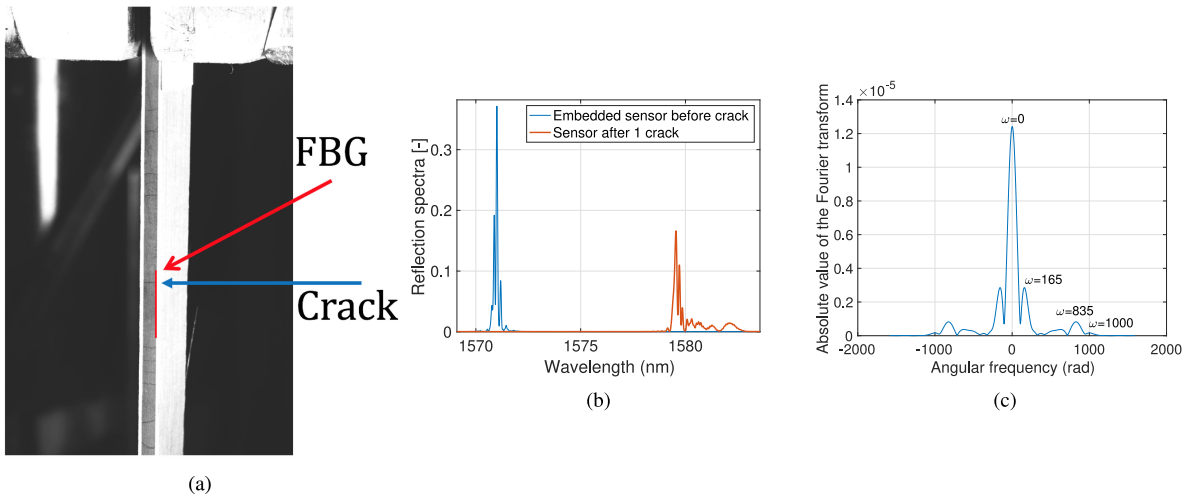

Fig. 6. (a): Carbon fibre specimen under a quasi-static tensile test, (b): Reflection spectra of the FBG before any cracks (blue) and after the formation of a crack (red), and (c): Fourier transform of the windowed side-lobes of the reflection spectrum.

V. Experimental Results and Discussion

In this section, we will validate our hypotheses using experimental measurements. For this purpose, we embedded FBG sensors within the layers of two different types of unidirectional (UD) composites. In the first example, we used AS4-UD carbon/Hexply 8552 prepreg sheets from Hexcel corporation, with the layup of $[0_4, 90_{16}, 0_4]$, and an FBG sensor with a length of $L = 10$ mm embedded between the 4th and 5th layer of the composite (at the interface of the 0° and 90° layers). We followed the curing process specified in the datasheet of the material. The FBG sensor was a DTG type sensor from the company FBGS, with a nominal Bragg wavelength of $\lambda_n = 1570$ nm. The DTG sensors had an Ormocer coating, which according to the producing company, allows a 1:1 strain transfer to the sensor. The mechanical and physical properties of the material are given in Table I. After the production, the specimens were cut into coupons of 2.5 by 15 centimetres, with the FBG at the centre of the coupon. The specimens were then subjected to a quasi-static test using a 100 kN MTS machine, where we increased the tensile stress from $\sigma = 50$ MPa to $\sigma = 400$ MPa in steps of $\Delta\sigma = 10$ MPa.

The FBG reflection spectra were recorded using a PXIe-4844 FBG interrogator from National Instruments, which has a dynamic range of 40 dB and a wavelength resolution of 4 pm. Also, in order to localise the cracks, we placed a camera facing the side of the specimens (therefore directly viewing the crack formation in the 90° layers of the composite, as seen in Fig. 6(a)). As expected from our model and the literature, before the formation of the cracks the FBG reflection spectrum held its general shape without much difference during the tensile test. It is noteworthy that since the curing of the carbon fibre panel was performed in an autoclave with pressures as high as 8 bar, there was already a residual transverse load on the FBG sensor. Therefore, even a sensor in an unloaded coupon was already affected by birefringence effects and widened reflection spectrum (widened by more than 2 times), and hence the asymmetrical shape of the sensor at the start of the experiment. Right after the formation of the first crack, the reflected spectrum changed shape and new harmonics were created. Fig. 6 shows the specimen under tensile testing, the FBG reflection spectrum before and after crack formation, and the emerged new harmonics in the Fourier transform of the side-lobes of the reflection spectrum. As seen from this figure, at this particular time during the test (at $\sigma = 330$ MPa), one single

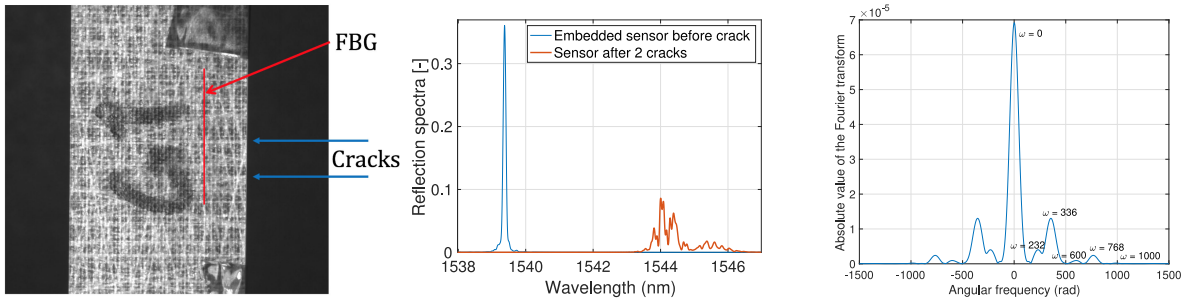

(a) (b) (c)

Fig. 7. (a): Glass fibre specimen under a quasi-static tensile test, (b): Reflection spectra of the FBG before any cracks (blue) and after the formation of two cracks (red), and (c): Fourier transform of the windowed side-lobes of the reflection spectrum.

crack was formed at location $z = 1.65$ mm from the start of the sensor, which results in the emergence of two additional peaks at $\omega = \{165, 835\}$ rad in the Fourier domain. The resulting new harmonics due to this crack are shown in Fig. 6(c), and it can be seen that they are located at the expected locations with respect to the location of the crack.

In the second experiment, we used UD glass fibre materials from Saertex GmbH, with a density of 228 g/m^2, a layup of $[0_2, 90_6, 0_2]$ and an overall thickness of 1.65 mm. The FBG sensors were embedded between the 2nd and the 3rd layers of the composite (again at the interface of the 0° and 90° layers). For this material, we used the fusion method to produce the composites, from Epikote 04908 resin and curing agent from Hexion Ltd. The material was initially cured at room temperature for 24 hours, and then for 6 hours in the oven at 80 °C and at a pressure of 1000 mbar. After the curing process, the specimens were cut into 3 by 25 centimetre coupons, with the FBG sensor at the centre of the coupon. For this example we also used a camera to record the crack formation, but since glass is translucent, the camera was facing the surface of the material, and we could see the cracks forming in the internal layers of the composite from the surface. The GFRP specimens were subjected to a similar test as the CFRP specimens, but starting at $\sigma = 10$ MPa to $\sigma = 150$ MPa in steps of $\Delta\sigma = 5$ MPa, as the GFRP specimens were less stiff than the CFRP specimens used in this study. Fig. 7 shows the specimen under tensile test at $\sigma = 50$ MPa, where two transverse cracks have already formed at locations $z = 6$ mm and $z = 7.68$ mm from the start of the sensor. The localisation of the cracks from the recorded images was performed by visually comparing consecutive images at different force loads. The FBG reflection spectra before and after crack formation, and the emerged new harmonics in the Fourier transform of the side-lobes of the reflection spectrum are also shown in this figure. Also note that since the sensor did not undergo high transverse pressures during its production, the FBG reflection spectrum looks more pristine and is less affected by birefringence effects. Given the locations $z = 6$ mm and $z = 7.68$ mm, we expect the emergence of additional peaks at $\omega = \{600, 768, 400, 232, 336\}$rad in the Fourier domain, which correspond well with the resulting peaks from the experiment. Note that in both experiments, since the number of cracks were limited to just 1 or 2, we could also localise the cracks. But having more than 2 cracks and having no access to the phase of the reflection spectrum will make their localisation much more difficult.

As it is evident from these experiments, our model could perfectly explain the emergence of the new peaks in the Fourier transform of the side-lobes of the reflection spectrum, and the peaky nature of the strain field due to the transverse cracks has a clear effect on these new harmonics. It can be also seen that birefringence effects and other noise sources did not affect the results. Note that the sensors used in these experiments were partially apodized, and hence, the lower amplitude of the $\omega = 1000$ peaks compared with the simulated examples.

As a last example, we tried to create a widened FBG reflection spectrum under a smooth non-uniform strain field, without having any cracks along the FBG length. We applied a three point bending test (loading pin on the sensor location) on one of the glass fibre specimens with an embedded FBG. Due to the non-uniformity of this strain field, the resulting reflection spectrum (shown in Fig. 8) became wider (the FWHM of an unstressed sensor was 84 pm, and it was widened by three times under the test), however, as seen from Fig. 8(b), no meaningful new harmonics have been added to the Fourier transform of the side-lobes of the reflection spectrum.

In summary, we argue that if there is a sudden change of strain distribution along the FBG length, it will have a direct effect on the reflection spectrum side-lobes. In this paper, we analysed this phenomenon in the formation of transverse cracks in unidirectional composite materials, but it can be extended to any other structure or material as well, including metals or concrete. The conditions that need to be met in order to perceive this effect are firstly, a direct contact of the sensor with the sharply varying strain field, and secondly, a high enough strain peak amplitude. The latter condition depends on the type of sensor in use, and also, the host material under investigation. For instance, in the glass fibre composite specimens with the given dimensions used in this study, and using DTG type sensors, computer simulations suggest that a strain peak of around 400 $\mu\epsilon$ will result in distinguishable new harmonics in the Fourier transform of the FBG reflection spectrum side-lobes, whereas for the carbon fibre specimens, this value was around 300 $\mu\epsilon$, which is due to the stiffer nature of the carbon fibre samples. With that in mind, it should be noted that in the laboratory experiments, the first cracks were

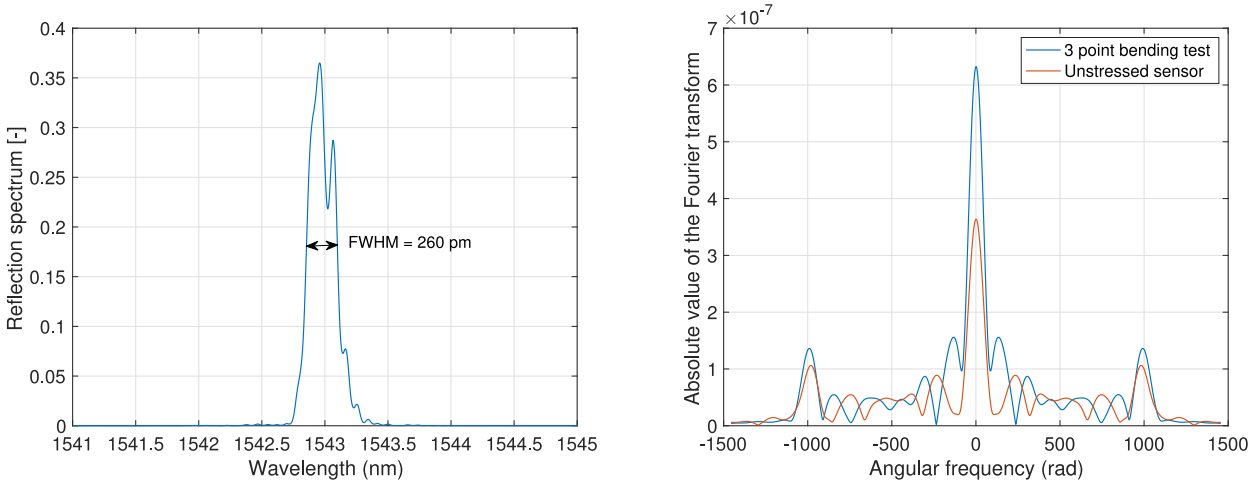

Fig. 8. (a): Reflection spectrum of an FBG under a three point bending test, (b): Fourier transform of the windowed side-lobes of the reflection spectra from the stressed and unstressed sensor.

forming under strain peak values of more than 1000 $\mu\epsilon$, which is already far more than the theoretical sensitivity threshold of the FBG sensors.

VI. Conclusions

In this paper we have demonstrated a clear relationship between the transverse cracks along the length of FBG sensors, and the emergence of new harmonics in the Fourier transform of the side-lobes of the FBG reflection spectra. We argued that the mere widening of the FBG reflection spectra is not a reliable measure for detection of cracks, as it might also occur in response to other types of non-uniform strain fields, and we suggested to focus on the information in the side-lobes of the reflection spectra as a more reliable indication of cracks along the sensor length. We validated our model with both computer simulations and experimental measurements, and the results were in good agreement with our model. Future works in this subject could include analysis of the crack formation in different layup configurations of composite materials, and their effects on the FBG reflection spectra. Also, extending the current model to the other types of damages in composite structures could also be beneficial to the community.

Acknowledgement

This research is part of the TKI Smart Sensing for Aviation Project, sponsored by the Dutch Ministry of Economic Affairs under the Topsectoren policy for High Tech Systems and Materials, and industry partners Airbus Defence and Space, Fokker Technologies-GKN Aerospace, Royal Schiphol Group, and by the H2020 project Extreme GA636549.

References

[1] A. D. Kersey *et al.*, "Fiber grating sensors," *J. Lightw. Technol.*, vol. 15, no. 8, pp. 1442–1463, Aug. 1997.
[2] Y.-J. Rao, "Recent progress in applications of in-fibre Bragg grating sensors," *Opt. Lasers Eng.*, vol. 31, no. 4, pp. 297–324, 1999.
[3] D. Kinet, P. Mégret, K. W. Goossen, L. Qiu, D. Heider, and C. Caucheteur, "Fiber bragg grating sensors toward structural health monitoring in composite materials: Challenges and solutions," *Sensors*, vol. 14, no. 4, pp. 7394–7419, 2014.
[4] S.-i. Takeda, Y. Aoki, and Y. Nagao, "Damage monitoring of CFRP stiffened panels under compressive load using FBG sensors," *Composite Struct.*, vol. 94, no. 3, pp. 813–819, 2012.
[5] N. Takeda, Y. Okabe, and T. Mizutani, "Damage detection in composites using optical fibre sensors," *Proc. Inst. Mech. Eng. Part G: J. Aerosp. Eng.*, vol. 221, no. 4, pp. 497–508, 2007.
[6] Y. Okabe, T. Mizutani, S. Yashiro, and N. Takeda, "Detection of microscopic damages in composite laminates," *Composites Sci. Technol.*, vol. 62, no. 7, pp. 951–958, 2002.
[7] T. Erdogan, "Fiber grating spectra," *J. Lightw. Technol.*, vol. 15, no. 8, pp. 1277–1294, Aug. 1997.
[8] Y. Okabe, R. Tsuji, and N. Takeda, "Application of chirped fiber Bragg grating sensors for identification of crack locations in composites," *Composites Part A: Appl. Sci. Manuf.*, vol. 35, no. 1, pp. 59–65, 2004.
[9] T. Okabe and S. Yashiro, "Damage detection in holed composite laminates using an embedded FBG sensor," *Composites Part A: Appl. Sci. Manuf.*, vol. 43, no. 3, pp. 388–397, 2012.
[10] A. R. Chambers, M. C. Mowlem, and L. Dokos, "Evaluating impact damage in CFRP using fibre optic sensors," *Composites Sci. Technol.*, vol. 67, no. 6, pp. 1235–1242, 2007.
[11] Y. Okabe, S. Yashiro, T. Kosaka, and N. Takeda, "Detection of transverse cracks in CFRP composites using embedded fiber Bragg grating sensors," *Smart Mater. Struct.*, vol. 9, no. 6, 2000, Art. no. 832.
[12] A. Rajabzadeh, R. Heusdens, R. C. Hendriks, and R. M. Groves, "Analysis of the side-lobes of FBG reflection spectra from matrix cracks in composites," in *Proc. 26th Opt. Fiber Sensors Conf.*, Lausanne, Switzerland, 2018, Paper TuE97.
[13] A. Rajabzadeh, R. Heusdens, R. C. Hendriks, and R. M. Groves, "Calculation of the mean strain of smooth non-uniform strain fields using conventional FBG sensors," *J. Lightw. Technol.*, vol. 36, no. 17, pp. 3716–3725, Sep. 2018.
[14] M. Yamada and K. Sakuda, "Analysis of almost-periodic distributed feedback slab waveguides via a fundamental matrix approach," *Appl. Opt.*, vol. 26, no. 16, pp. 3474–3478, 1987.
[15] L. McCartney, "Theory of stress transfer in a 0-90-0 cross-ply laminate containing a parallel array of transverse cracks," *J. Mech. Phys. Solids*, vol. 40, no. 1, pp. 27–68, 1992.
[16] J.-M. Berthelot, "Transverse cracking and delamination in cross-ply glass-fiber and carbon-fiber reinforced plastic laminates: Static and fatigue loading," *Appl. Mech. Rev.*, vol. 56, no. 1, pp. 111–147, 2003.
[17] A. V. Oppenheim, *Discrete-Time Signal Processing*. New Delhi, India: Pearson Education India, 1999, pp. 468–471.
[18] T. M. Hermann, J. E. Locke, and K. K. Wetzel, "Fabrication, testing, and analysis of anisotropic carbon/glass hybrid composites volume 1: Technical report," Tech. Rep., Sandia National Laboratories, 2006.